ACS APPLIED ENERGY MATERIALS

www.acsaem.org Article

Performance Limitations of CaCoSO as a Positive Electrode Material for Calcium Storage

Da Tie,[§] Petru Apostol,[§] Mengyuan Du, Zhao Li, Xiaodong Lin, Shubhadeep Pal, Robert Markowski, Xiaolong Guo, Hewei Xu, Andrii Kachmar, Vasudeva Rao Bakuru, Darsi Rambabu, Yinghui Zhang, Fang Xia, Yaroslav Filinchuk, Jean-François Gohy, and Alexandru Vlad*

Cite This: https://doi.org/10.1021/acsaem.4c03288 Read Online

ACCESS | Metrics & More | Article Recommendations | Supporting Information

ABSTRACT: Calcium metal batteries (CMBs) are promising candidates for next-generation electrochemical energy storage systems due to their high volumetric capacity, abundance, sustainability, and safety. Recent DFT predictions suggested that the layered CaCoSO phase can enable sequential Co^{2+}/Co^{3+} and Co^{3+}/Co^{4+} redox activity at an average potential of 2.8 V vs Ca^{2+}/Ca, making it a promising candidate for high-energy-density CMBs [Torres, A. et al. *Chem. Mater.* **2021**, *33*(7), 2488−2497]. Inspired by these metrics, in this work, we present the synthesis and electrochemical analysis of the CaCoSO phase. Theoretical capacity can be extracted through galvanostatic cycling, albeit accompanied by high polarization. *In situ* XRD and DEMS analyses, however, reveal that the capacity arises primarily from a combination of material decomposition and electrolyte degradation rather than reversible Ca^{2+} ion storage. The apparent discharge capacity is attributed to the cathodic decomposition of generated water during the subsequent anodic step, making the overall electrochemical process appear as reversible. This work underscores the complexity of achieving stable calcium-ion storage and aligns with similar challenges reported for other systems, highlighting the need for realistic testing conditions and providing critical insights to guide the development of advanced electrode materials and electrolytes for CMBs.

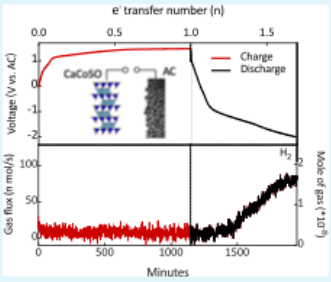

KEYWORDS: *calcium metal battery, calcium-ion storage, positive electrode material, layered materials, electrocatalysis*

This manuscript is a preprint of an article published in *ACS Applied Energy Materials, ACS*.

DOI : 10.1021/acsaem.4c03288

The final authenticated version is available online at :

https://pubs.acs.org/doi/10.1021/acsaem.4c03288

Performance Limitations of CaCoSO as a Positive Electrode Material for Calcium Storage

Da Tie[‡,a], *Petru Apostol*[‡,a], *Mengyuan Du*[a], *Zhao Li*[a], *Xiaodong Lin*[a], *Shubhadeep Pal*[a], *Robert Markowski*[a], *Xiaolong Guo*[a], *Hewei Xu*[b], *Andrii Kachmar*[a], *Vasudeva Rao Bakuru*[a], *Darsi Rambabu* [a], *Yinghui Zhang*[a], *Fang Xia*[a], *Yaroslav Filinchuk*[a], *Jean-François Gohy*[a] & *Alexandru Vlad*[*a]

[a] Institute of Condensed Matter and Nanosciences, Molecular Chemistry, Materials and Catalysis, Université catholique de Louvain, Louvain-la-Neuve B-1348, Belgium.

[b] Taiyuan Institute of Technology, Department of Materials Engineering, Taiyuan, 030008, China.

‡ These authors contribute equally to this work.

[*]Email: alexandru.vlad@uclouvain.be

KEYWORDS

Calcium metal battery, Calcium-ion storage, Positive Electrode Material, Layered Materials, Electrocatalysis.

ABSTRACT

Calcium metal batteries (CMBs) are promising candidates for next-generation electrochemical energy storage systems due to their high volumetric capacity, abundance, sustainability, and safety. Recent DFT predictions suggested that the layered CaCoSO phase can enable sequential Co^{2+}/Co^{3+} and Co^{3+}/Co^{4+} redox activity at an average potential of 2.8 V vs. Ca^{2+}/Ca, making it a promising candidate for high-energy-density CMBs. (Torres, A.; Casals, J. L.; Arroyo-de Dompablo, M. E. Chem. Mater. 2021, 33 (7), 2488–2497.) Inspired by these metrics, in this work we present the synthesis and electrochemical analysis of the CaCoSO phase. Theoretical capacity can be extracted through galvanostatic cycling, albeit accompanied by high polarization. *In situ* XRD and DEMS analyses, however, reveal that the capacity arises primarily from a combination of material decomposition and electrolyte degradation rather than reversible Ca^{2+} ion storage. The apparent discharge capacity is attributed to cathodic decomposition of generated water during the subsequent anodic step, making the overall electrochemical process appear as reversible. This work underscores the complexity of achieving stable calcium-ion storage and aligns with similar challenges reported for other systems, highlighting the need for realistic testing conditions and providing critical insights to guide the development of advanced electrode materials and electrolytes for CMBs.

INTRODUCTION

The necessity to innovate and develop alternatives to lithium-ion batteries (LIBs) has become increasingly important due to the limited availability of required raw materials, rising production costs, and significant issues related to safety and environmental sustainability.[1,2] The finite supply of lithium and other key components, coupled with their geographically constrained distribution, further exacerbates the resources scarcity problem. Moreover, the increasing demand for LIBs in various applications, from consumer electronics to electric vehicles, drives up costs and intensifies the competition for these materials. Additionally, the inherent safety risks associated with LIBs, including thermal runaway and potential for fires, alongside the environmental impact of their production and disposal, underscore the urgent need for sustainable and safer energy storage alternatives. Consequently, research and development efforts have been intensifying to identify and commercialize viable alternative technologies that can overcome these challenges and meet the growing global energy demand.[3,4]

While much research has centered on lithium-based systems like Li-S and Li-air (O_2) batteries,[5] recent studies have explored the utility of divalent metals such as calcium (Ca) in CMBs.[6,7] Calcium is the 5th most abundant in the Earth's crust, offering cost-effective raw materials for metal-based batteries.[8,9] Since calcium ions can undergo a two-electron redox process at a redox potential close to Li metal, CMBs could theoretically achieve high specific capacity and energy density, if a suitable cathode material is successfully identified and all

current associated challenges are solved. Recent advancements have demonstrated electrolytes capable of enabling calcium plating and stripping, showing promise for CMB development.[10–12] Complementary, certain progress on positive electrode materials has been also attained, with layered vanadate phases, Prussian blue, polyanion compounds, sulfur/sulfides and organic materials showing steady progress.[13–18] However, these materials still face limited performance for Ca-storage, with limited capacity, poor capacity retention and slow kinetics.

The development of high-performance electrode materials for CMB, and in general for divalent metal batteries, faces three main challenges. (i) Traditional materials applied for monovalent ion storage (e.g., Li-ion, Na-ion, or metal versions) are thermodynamically and crystallographically unsuitable due to divalent intercalants requiring higher coordination numbers, which disrupt ion diffusion and battery performance.[19,20] (ii) Divalent intercalants display stronger (than monovalent for instance) electrostatic interactions with the host framework, leading to slow kinetics and high charge-discharge hysteresis (*e.g.* polarization).[21,22] For example, layered metal oxides, despite being best candidates for monovalent cation storage, exhibit a high migration barrier for divalent ions, impeding room-temperature efficient opperation.[23] (iii) Intercalation of divalent ions can cause structural or volume changes, leading to structural defects and degradation.[24,25] For CMBs to advance and achieve practical development, it remains thus essential to develop new positive electrode materials and phases that offer practical charge storage performances and metrics.

Recently, computational studies, particularly using Density Functional Theory (DFT), have become vital in identifying potential electrode materials for batteries, including also for Ca-

ion storage.[26] DFT enables the exploration of both existing and hypothetical material phases.[27] It provides comparative studies of potential electrode materials for calcium-based (but not only) batteries, focusing on intercalation voltage, migration barrier, and phase stability — aspects that would nevertheless require experimental validation.[22,28] For example, materials such as $Ca_2MnO_{3.5}$,[29] CaV_2O_4,[29] and $Ca_4Fe_9O_{17}$[30] have been predicted to have ability to extract Ca^{2+} or support reversible reactions, being subsequently synthesized and tested for Ca^{2+} extraction/intercalation performances. However, experimental findings do not always align with the computational predictions. Despite these discrepancies, the extensive range of materials identified by DFT offers significant opportunities for further experimental research and potential breakthroughs in the development of calcium-based batteries.

Torres et al.[31] expanded the investigation of materials for Ca positive electrode materials applications using DFT, incorporating crystal chemistries based on various anions: nitrides, oxysulfides, pyrophosphates, and phosphates. Their research aimed to identify stable compounds, focusing exclusively on phases listed in the Inorganic Crystal Structure Database (ICSD) rather than on hypothetical virtual materials. One intriguing material under their investigation was CaCoSO, assessed for its suitability as a positive electrode for calcium storage. Its low molar mass enhances its theoretical specific capacity to 365 mAh g^{-1}, particularly noteworthy due to the possible sequential Co^{2+}/Co^{3+} and Co^{3+}/Co^{4+} redox couples, giving access to a 2-electrons, equivalent of one Ca^{2+}, redox exchange. One has to note that anion redox of O^{2-} or S^{2-} is not to be excluded, with also, as noted by the authors, possible degradation of the material, despite oxy-sulfide phases shown to be stable for example for Li-ion storage.[32–36]

Furthermore, the predicted voltage range was compatible with existing electrolytes used at room temperature, making it a promising candidate for facilitating the intercalation and extraction of calcium ions.

Considering these promising metrics, in this study we synthesized, characterized and investigated the respective CaCoSO phase, with a focus on Ca^{2+} release and storage capability. This approach seeking to bridge the gap between theoretical potential and practical application in the development of efficient calcium-based batteries. Electrochemical testing has revealed apparent full Ca-ion extraction and insertion, albeit proceeding with a large polarization between the charge and discharge steps, as already noted for other reported Ca-ion host materials. Careful analysis however revealed that the CaCoSO material does not undergo a phase change upon Ca-extraction but instead undergoes gradual decomposition during the charge process. Capacity limited cycling and *in situ* XRD revealed that the irreversible changes occur from the early stages of Ca^{2+} extraction with no signatures of solid-solution or biphasic progress of the reaction. Analysis using the Differential Electron Mass Spectrometer (DEMS) indicated that the observed galvanostatic charge-discharge plateaus are due to a combination of anodic decomposition of CaCoSO accompanied by catalytic degradation of the electrolyte, followed by the decomposition of water by-product generated from previous cycles during the discharge step. The analyzed suitability of CaCoSO as positive electrode material for calcium-based batteries highlights the challenges associated with efficient Ca-ion extraction and insertion hosts, and the need for future studies to consider the influence of side reaction-generated galvanostatic charge-discharge artifact plateaus, as similar phenomena can be

occasionally noted in related research and assigned to efficient divalent cation (Mg^{2+} or Ca^{2+}) storage.

EXPERIMENTAL SECTION

The synthesis of CaCoSO entailed the utilization of CaO (Sigma-Aldrich 99.9%), Co (Sigma-Aldrich 99.9%), and S (Sigma-Aldrich 99.98%). Stoichiometric amounts of the CaO, Co, and S powders were first grinded and sealed within evacuated quartz ampoules. The initial phase of the thermal treatment was conducted at a heating ramp of 2 °C min^{-1} to promote the reaction of elemental sulfur, while preventing the development of undue overpressure. The thermal procedure involved maintaining the reactants at 900 °C for two periods of 48 hours each, with an intermediate step in which the material was re-ground to ensure uniformity. Following these heating cycles, the synthesized product was subjected to fine grinding under an inert argon atmosphere inside a glovebox to prevent contamination and degradation.

PXRD was performed using a STOE DARMSTADT Stadi P transmission diffractometer operated with Mo anode (Kα radiation, λ = 0.7093 Å). Indexing and refinement of the PXRD datasets was conducted using the FullProf Suite software. Morphological characterization was performed using Scanning Electron Microscopy (SEM, ZEISS AURIGA FIB-SEM) with an integrated Energy Dispersive Spectroscopy (EDS) module for elemental composition analysis. Quantitative elemental composition analysis was performed via ICP-OES on a Perkin Elmer Avio 220 Max system.

The construction of the working electrodes was typically done by dry grinding a homogenous composite electrode of CaCoSO active material powder (50 wt.%), Super P carbon (SP) as a conductive additive (40 wt.%), and 10 wt.% polytetrafluoroethylene (PTFE, powder, Sigma-Aldrich) as a binding agent. The resultant composite was compacted onto CR2032 coin cell casings (SS-316 steel) to attain a mass loading of 8-12 mg cm-2. Electrochemical evaluation was carried out in half-cell configuration (CR2032, SS316). In the case of Lithium cells, metallic Li chips served as both the counter and the pseudo-reference electrode, separated by a Whatman glassfiber membrane (GF/D). Electrolyte LP57 was formulated with 1.2M LiPF6 in a 3:7 volumetric ratio of ethylene carbonate (EC) and ethyl methyl carbonate (EMC), whereas LP30 consisted of 1M LiPF6 in a 1:1 volumetric ratio of EC and dimethyl carbonate (DMC). Additional electrolyte systems referenced in the manuscript were also tested. For Calcium-ion storage cells, activated carbon (AC) cloth was used as both counter and pseudo-reference electrode, with a similar Whatman glassfiber (GF/D) used as separator. The Ca-ion electrolytes tested included 0.5M $Ca(TFSI)_2$ in a 1:1 volumetric ratio of EC:PC, 0.5M $Ca(TFSI)_2$ in Diglyme (G2), or 0.5M $Ca(BH)_4$ in Tetrahydrofuran (THF). Cell assembly was performed in an argon-filled glovebox (MBraun, <1 ppm O_2 and H_2O). Galvanostatic cycling was conducted at 25°C using Neware battery cycler.

The use of AC counter and pseudo-reference electrode was imposed by the difficulty of achieving a stable and reliable Ca-metal electrode. After a resting of 12h, the OCV of the constructed cells relative to AC typically stabilized at -0.2V, while in house experience indicates that the OCP of AC is around 2.8V vs. Ca/Ca^{2+}. It has to be noted that these values

may vary for different electrolytes, type of AC, or cell construct. The capacity ratio of AC to CaCoSO (active used) was typically in the range of 2 to 10, depending on the cycling conditions used (limited, full capacity) and cell type (galvanostatic cycling cells, DEMS or electrolyte analysis open cells).

For the GITT tests, a CaCoSO - AC cell was assembled with 0.5M $Ca(TFSI)_2$ in a 1:1 volumetric ratio of EC:PC as electrolyte. The cell was galvanostatically charged at a rate of 0.02C (1C rate being equivalent of 365 mA g-1, or $2e^-/1Ca^{2+}$ exchanged in 1 hour) for periods of 60 min, followed by open-circuit relaxation periods for a duration of 12 hours (Figure 2b). The curves resemble those seen in the galvanostatic charge-discharge data shown in Figure 2a. Under near-equilibrium conditions, 0.5 e^- / 0.25 Ca^{2+} equivalent capacity was cycled.

In situ XRD patterns were acquired with a STOE Stadi P diffractometer equipped with Mo anode (Kα radiation, λ = 0.7093 Å), and operated in transmission mode. Electrode preparation mirrored the procedure utilized for the electrochemical tests. The details for cell fabrication are presented in Supplementary Figure S5.

ICP-OES analysis was conducted to evaluate changes in the electrolyte composition. The electrode powder was prepared following the same procedures as described in the electrochemical tests, by compressing the powder into a stainless-steel gauge. For Li-cells, the electrolyte used was LP57, with CaCoSO serving as the working electrode and activated carbon (AC) as both the counter and pseudo-reference electrode. For Calcium-ion storage cells, the electrolyte consisted of 0.5M $Ca(TFSI)_2$ in a 1:1 EC:PC mixture, with CaCoSO as the working electrode and AC as both the counter and pseudo-reference electrode. Detailed description of

the cell configuration for the ICP-OES analysis experiments is provided in Figures S10 and S11. The electrolyte was extracted at the specified potentials for subsequent elemental analysis.

DEMS analysis was conducted to monitor the gas evolution during the initial charging and discharging cycles. The electrode material was processed in the same manner as for electrochemical testing, by compressing it into a stainless-steel mesh. For the Li-cell configuration, the electrodes were incorporated into electrochemical cells (EC-cells) with metallic lithium serving both as the counter and pseudo-reference electrode, and LP57 as the electrolyte. In the Calcium-ion storage setup, activated carbon (AC) functioned as both the counter and reference electrode, with a 0.5M solution of 0.5M $Ca(TFSI)_2$ in a 1:1 EC:PC mixture used as the electrolyte. The cells were then interfaced with the mass spectrometer, which was constantly flushed with argon. This setup allowed for the transfer of gases from the cell directly to the mass spectrometer, where mass spectral data were correlated in time function of the cell voltage. Ion current intensities were finely tuned to selectively record mass-to-charge (m/z) ratios of 2, 32, and 44.

Chemical oxidation procedure involved the dispersion of the CaCoSO in a NO_2BF_4 solution using acetonitrile (ACN) as the solvent at molar ratios of 1:1 and 1:4. This mixture was subjected to reflux for a duration of 6 hours. An inert atmosphere was sustained by continuous bubbling of argon gas, which also facilitated the removal of NO_2 gas, a byproduct of the reaction. Upon completion of the oxidation process, the products were washed with anhydrous diethyl ether, followed by drying, and then collected for subsequent XRD characterization.

RESULT AND DISCUSSION

The CaCoSO was synthesized through a solid-state reaction following the procedure reported by Salte et al.[37] The structure was refined using the Rietveld method, and the majority of peaks were indexed to $P6_3/mc$ space group characteristic of CaCoSO structure (**Figure 1a, Table S1 & S2**). A trace amount of Co_9S_8, comprising approximately 1.2% of the total molar content was also identified, belonging to the cubic crystal system with space group $Fm\text{-}3m$. The structural configuration of CaCoSO consists of alternating layers oriented along the [001] direction: a layer composed of $CoOS_3$ tetrahedra and with calcium ions located in the interlayer (**Figure 1b**). Each $CoOS_3$ tetrahedron, constructed from three S^{2-} in the *ab* plane and an additional apical O^{2-}, shares all its S^{2-} with two neighboring $CoOS_3$ tetrahedra, thus forming a triangular cobalt network. Within this framework, Ca^{2+} are coordinated by three S^{2-} and three O^{2-}, forming edge-shared octahedral blocks. Scanning electron microscopy images reveal non-regular micrometer-sized particles of the material (**Figure 1c, left**), and energy-dispersive spectroscopy elemental mapping confirmed a uniform distribution of Ca, Co, O, and S in CaCoSO (**Figure 1c, right**).

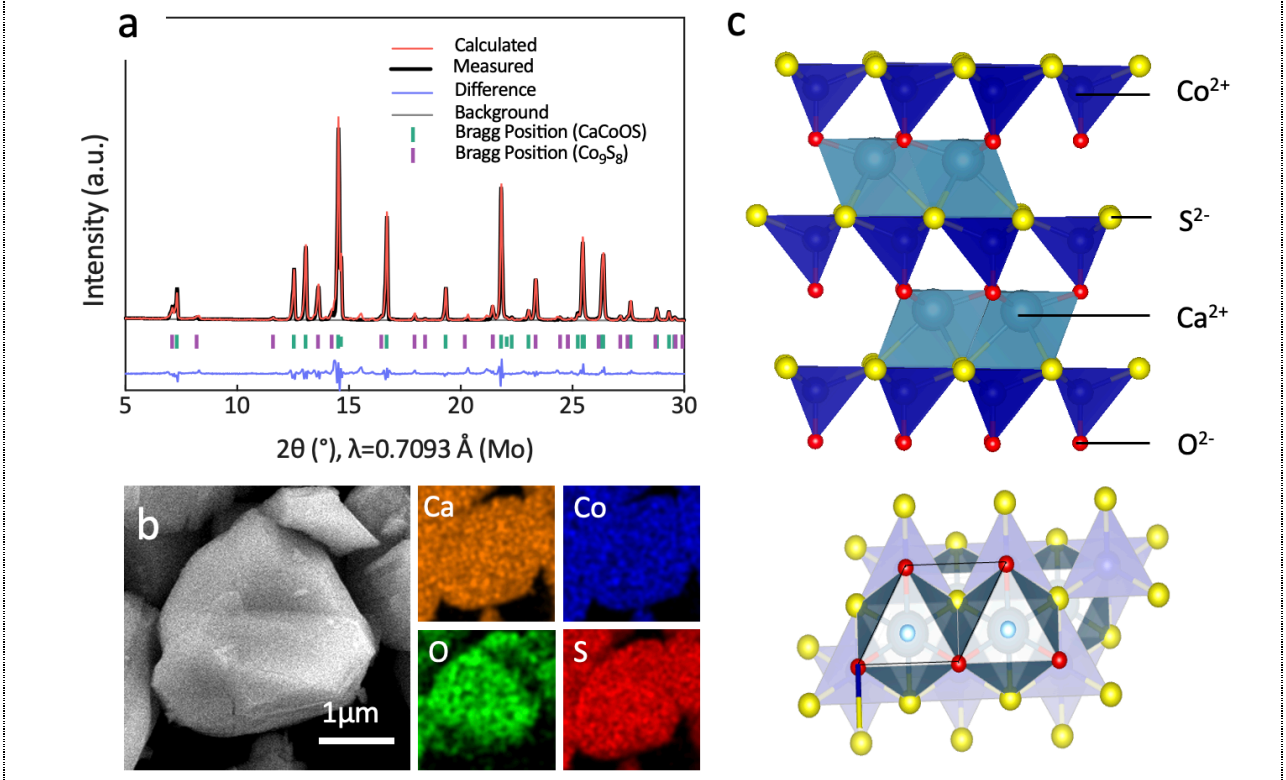

Figure 1. (a) The Rietveld refinement of X-ray diffraction data of CaCoSO; (b) SEM image of as synthesized CaCoSO particles with the corresponding energy-dispersive X-ray elemental mapping showing uniform distribution of elements; (c) The crystal structure of CaCoSO viewed along a (top) and c axis (bottom).

To assess the electrochemical activity of CaCoSO, experiments were first conducted to extract and insert Ca^{2+} using CaCoSO as the positive electrode material and activated carbon (AC) as the counter and pseudo-reference electrode (denoted hereafter as CaCoSO-AC), using 0.5M $Ca(TFSI)_2$ in EC/PC (1:1) as electrolyte. Various charge and discharge states were accessed, according to equivalent amounts of 0.5 / 1 / 1.5 e^- (corresponding to $0.25Ca^{2+}$ / $0.5Ca^{2+}$ / $0.75Ca^{2+}$) extracted at a rate of 0.05C (1C rate corresponds to 365 mA g^{-1}, or 1 Ca^{2+} exchanged in one hour). The capacity being deliberately limited to circumvent potential adverse effects of

for example full Ca^{2+} extraction on the framework stability (**Figure 2a**). A distinct electrochemical response apparent to Ca^{2+} extraction can be noted during the charging step, characterized by a voltage-capacity plateau onset at approximately 0.8V *vs* AC, with the following discharge process featuring an immediate plateau starting at -1V vs. AC. This behavior was consistent across different electrolyte formulations tested (**Figure S1**), with however characteristics specific to the electrolyte composition. Consequently, the CaCoSO-AC cells were cycled with capacity limitations of equivalent amounts 0.5 and 1 e^- (corresponding to 0.25 Ca^{2+} and 0.5 Ca^{2+}), as shown in **Figures 2b** and **2c**, respectively. When the capacity was limited to 0.5 e^-, CaCoSO-AC cells were able to sustain 100 cycles, despite the increasing polarization with successive cycles noted, a trend that persisted during the discharge phase. Interestingly, with a higher material utilization of $1e^-$ / ½ Ca^{2+} exchange, the CaCoSO-AC barely sustained 10 cycles (**Figure 2c**).

To further investigate the reversibility of CaCoSO during charge and discharge processes, the electrode charge and mass transfer kinetics were analyzed using the galvanostatic intermittent titration technique (GITT) (**Figure 2d**, details provided in the Supporting Information and related text, voltage vs. time plot provided in **Figure S2**, the relationship between time and cell potential for a single titration step in the GITT experiments shown in **Figure S3)**. The variation in intensity of polarization occurs during the whole process of both charge and discharge processes, with the voltage drop observed during the relaxation of anodic step being markedly smaller than during the cathodic step. Although the large overpotential observed in the GITT experiment indicates significant electrode polarization and suggests that

the reaction kinetics might be limited by either low electronic conductivity or slow Ca-ion diffusion, the inconsistency in voltage changes during the relaxation process reveal that the anodic and cathodic reactions are asymmetrical (*i.e.* fast extraction, slow insertion, or accompanying phase change).

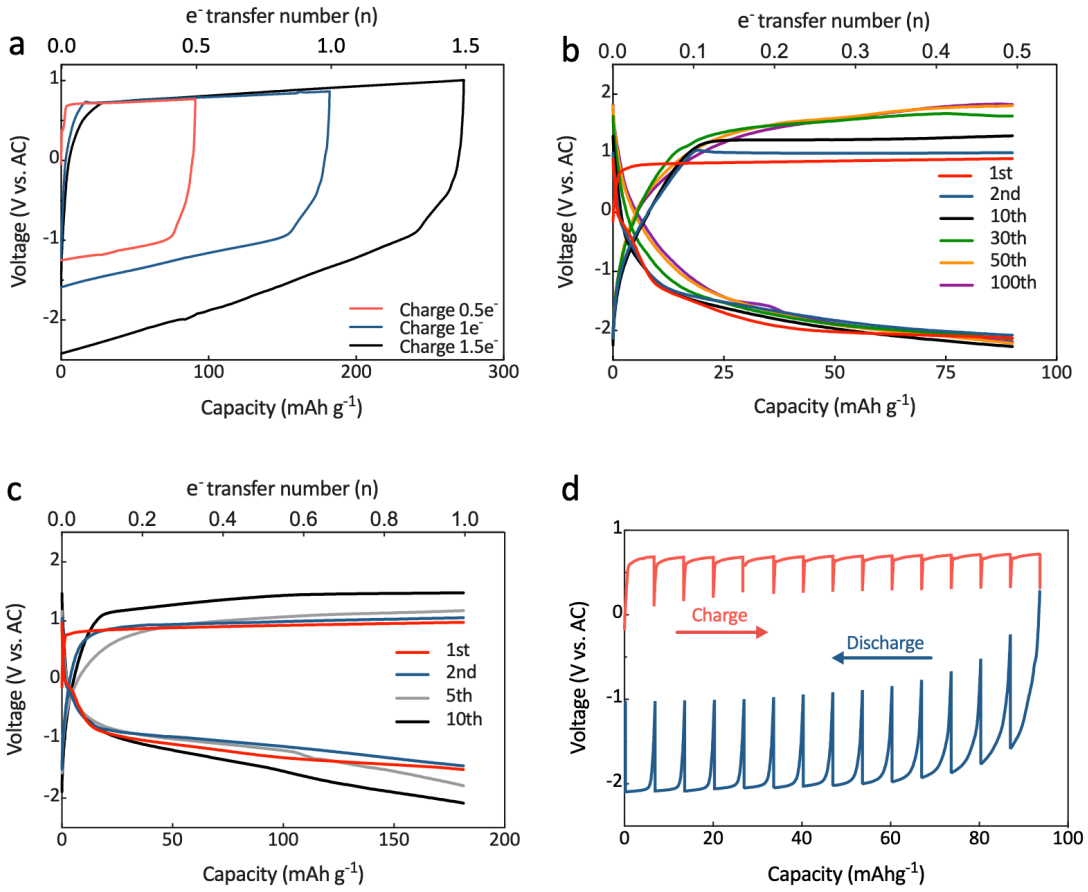

Figure 2. (a) Galvanostatic voltage vs. capacity curves acquired at a rate of 0.05C for CaCoSO-AC cells by limiting the extracted capacity at 0.5/1/1.5 e^- – 0.25/0.5/0.75 Ca^{2+} per equivalent of formula unit (where a 1C rate corresponds to 365 mA g^{-1}, or 1 Ca^{2+} exchanged in one hour); (b, c) Galvanostatic charge-discharge profiles of CaCoSO-AC cells with limited capacity at 0.5 e^- – 0.25 Ca^{2+} and 1 e^- – 0.5 Ca^{2+} per equivalent of formula unit, respectively. (d) First cycle GITT data for CaCoSO, tested with a current pulse step at a rate of 0.02C for a duration of 1 h, followed by relaxation at an open circuit for 12 h at each step. $Ca(TFSI)_2$ in EC/PC(1:1) was used as electrolyte.

To further explore whether the CaCoSO extracts Ca-ions during charging, electrochemical cells with varying components were assembled in half cell configuration using Li as negative electrode (denoted hereafter as CaCoSO-Li) using LP57 as electrolyte and the galvanostatic charge–discharge profiles were analyzed (**Figure 3**). To eliminate the influence of each component, different cell configurations were assembled, with the composition and schematic diagrams shown in **Figure 3a**. As a control experiment, we first tested a cell without any active material, consisting solely of a stainless steel (SS) plate in direct contact with the separator, resulting in negligible capacity during the charging step (**Figure 3b, cell 1**). Subsequently, we coated the SS with a slurry of PTFE and Super P (SP) (**Figure 3b, cell 2**). The results of cell 2 were very similar to cell 1, with the increase in capacity attributed to the larger surface area of the PTFE - SP electrode compared to only SS, and thus higher anodic decomposition current of electrolyte, or corrosion. These control experiments suggest that minimal electrolyte decomposition or corrosion occurs when using the LP57 electrolyte. The addition of CaCoSO to the electrode, either directly in contact with the SS gasket or by first coating onto a carbon-coated aluminum current collector, markedly altered the cycling profile. A consistent charge plateau was observed with no significant increase in potential, around 4V (**Figure 3c, cells 3** and **4**) with unexpectedly, more than 2-electrons being also possible to extract. The continued plateau suggested that the total capacity was not solely dependent on the Ca^{2+} extraction from CaCoSO phase, since the charging capacity exceeded the theoretical capacity. Additional tests in alternative electrolytes, including ionic liquids (**Figure S4**) confirmed the occurrence of this theoretical capacity exceeding process rather than continuing raising potential, suggesting that

the Ca^{2+} pseudo-release and storage behavior observed in the CaCoSO-AC/Li cells is largely driven by side reactions, with minimal corrosion of current collector and subsequent cycling of released species as suggested recently in the case of Mg-based systems.[38]

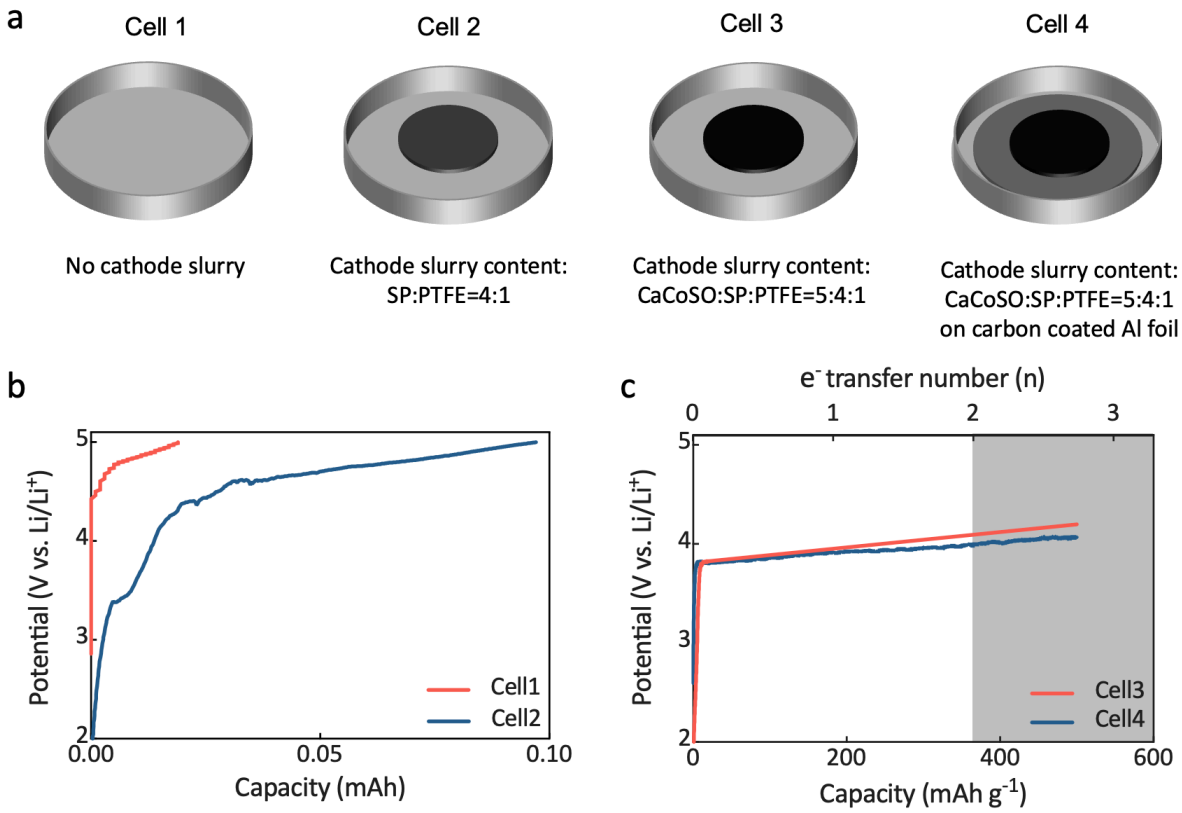

Figure 3. (a) Schematic diagram of the positive electrode composition of different control cells; (b) and (c) Galvanostatic potential *vs.* capacity curves acquired at a rate of 0.05C for Cells 1-4 (where a 1C rate corresponds to 365 mA g^{-1}, or 1 Ca^{2+} exchanged in one hour), the portion exceeding the theoretical capacity has been highlighted with a gray background in the figures. The cells configuration was CaCoSO-Li, with Li counter and pseudo-reference electrode, and LP57 as electrolyte.

Intrigued by these results, additional tests were performed to determine the source of this electrochemical response. First, the structural evolution of CaCoSO electrodes in CaCoSO-Li cell was examined through *in situ* XRD, experimental configuration being detailed in **Figure**

S5. In the XRD survey depicted in **Figure 4**, we identified characteristic peaks corresponding to CaCoSO alongside those of the Cu and Al current collectors from the *in situ* cell construct. Upon anodic polarization, the *in situ* XRD analysis reflected approximately 1/3rd intensity loss of the CaCoSO reflections peaks after an excess 3e$^-$ charging, with part of the electrode material being thus preserved. This indicates the occurrence of significant side reactions rather than complete structural degradation. No significant shifts in peak positions or the emergence of new peaks were observed (expected to accompany a biphasic or a solid-solution reaction). Comparative analysis revealed that the intensity for Cu(111) and Al(100) remained constant, confirming the absence of substantial chemical reactions within these components or XRD measurement artefacts (**Figure 4b & S6**). Also, there is no substantial change in the particle morphology indicated by the SEM image post-charging, which showed the material maintained the initial shape, with nevertheless the appearance of cracks (**Figure S7**). Considering these, it is reasonable to assume that the observed anodic plateau might not derive solely from the Ca^{2+} extraction from CaCoSO and associated material degradation. *Ex situ* XPS analysis of the charged samples (by 3-electrons) revealed a characteristic to SO_3^{2-} specie peak at 168 eV, indicating that the sulfur in CaCoSO is undergoing considerable oxidation upon charging process (**Figure S8**).

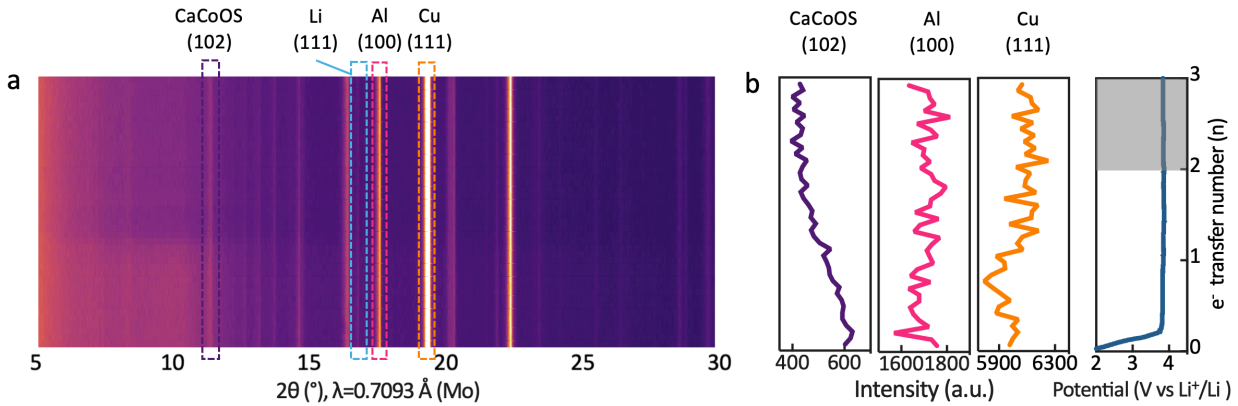

Figure 4. *In situ* XRD survey of the first charge cycle for CaCoSO displayed in 2-D contour plots (a) and the intensity evolution of the Cu (111), Al (100), and CaCoSO (102) diffraction planes with corresponding charge profile displayed to the right (b). Galvanostatic potential *vs.* capacity curves acquired at a rate of 0.05C (where a 1C rate corresponds to 365 mA g^{-1}, or 1 Ca^{2+} exchanged in one hour), the portion exceeding the theoretical capacity being highlighted with a gray background. The cell configuration was CaCoSO-Li, with Li counter and pseudo-reference electrode, and LP57 as electrolyte.

To determine whether partial or fully calcium depleted [Ca_0]CoSO phase can exist, and asses its stability, chemical oxidation of CaCoSO using different equivalent amounts of NO_2BF_4 was performed.[39,30] The results are shown in **Figure S9**. The reaction with 1 equivalent of NO_2BF_4 (corresponding to a $1e^-$oxidation) resulted in minor changes from the pristine phase, with the appearance of a new peak at 17° (**Figure S9**). The addition of 4 equivalents of NO_2BF_4 however led to complete decomposition, with only the Co_9S_8 phase detected (**Figure S9**). Further analyses using Inductively Coupled Plasma - Optical Emission Spectrometry (ICP-OES) of the supernatant after the chemical oxidation confirmed the presence of both Ca and Co ions (**Table S3**). Notably, the concentrations of Ca and Co were significantly higher in the solution when 4 equivalents of NO_2BF_4 was used, indicating the material decomposed followed by dissolution

of the species into the acetonitrile solvent. This implies that the calcium depleted [Ca_0]CoSO phase is unstable, and that CaCoSO degrades and releases soluble species in the electrolyte continuously during both chemical and electrochemical oxidation processes. However, it is important to emphasize that this decomposition may not be assigned as the primary mechanism driving the electrochemical oxidation process of the material as even after excess galvanostatic electrode oxidation, a part of the active material is preserved as noted from the *in situ* XRD analysis (**Figure 4**).

Considering these findings, additional experiments were conducted to identify the nature of the side reactions induced by the electrode-electrolyte interface, employing ICP-OES analysis to monitor changes of the elemental content in the electrolyte during the charge process (**Figure S10**). A minor increase in Ca and Co content was observed in the electrolyte collected at the end of the charge (**Table S4**), which aligns with gradual material decomposition, as confirmed from the chemical oxidation experiment analysis. The Fe content remained low, further supporting minimal stainless-steel current collector corrosion (**Figure 3a**). In previous research by Lipson et al. [40], evidence suggested that current collector corrosion could be a contributing factor to the abnormal charging curves observed in calcium-ion cells. However, this phenomenon was not detected in the CaCoSO-Li system, indicating that current collector stability may not be a concern in this specific configuration, or within the used voltage range.

As shown in **Table S4**, the lithium content of electrolyte increased markedly during the charging process, rising from 6215 ppm to 8903 ppm. Although some electrolyte evaporation was expected due to the lack of strict sealing in this particular cell assembly (**Figure S10**), the

observed electrolyte depletion rate was significantly higher than anticipated. Under normal conditions, the lithium content in the electrolyte would remain constant during this process since no other Li-sources were present in the system. This increase suggests that the electrolyte was being consumed, indicating the possibility of catalytic decomposition of the electrolyte (along with partial solvent evaporation not to be excluded, mainly of EMC component, b.p. 101°C).

Consequently, we employed differential electrochemical mass spectrometry (DEMS) to analyze the decomposition products during cycling in the CaCoSO-AC cell configuration employing LP57 as electrolyte. **Figure 5** shows the galvanostatic charge curve along with the gas generation rate of mass spectrometry measurements for CO_2 at m/z = 44 and O_2 at m/z = 32. Throughout the charging process, a steady release of O_2 and CO_2 is detected. Based on electrochemical and chemical oxidation result analysis discussed earlier, it has been established that CaCoSO undergoes gradual decomposition during charging, converting to Co_9S_8, suggesting that the primary source of oxygen evolution may originate from this process. Although oxygen may also arise from the oxidation of carbonates formed by the reaction of CO_2 with metal oxides, distinguishing between these pathways remains challenging.[41,42] It can be also noted that the release trend of CO_2 is similar to that of O_2, with a continuous and stable generation of CO_2 from the early stages of charging. This indicates that CaCoSO, or the generated decomposition products, also catalyze the decomposition of carbonate solvents contained in the electrolyte, inducing their breakdown at potential of 4V (*vs.* Li^+/Li). This is unusually low, given the widely accepted anodic stability of carbonate electrolyte formulations

of up to 4.5V (*vs.* Li^+/Li).[43] Therefore, the catalytic decomposition of the electrolyte and the decomposition of the material itself occur simultaneously, collectively leading to the apparent charging plateau observed in the CaCoSO-based cells during the charging process.

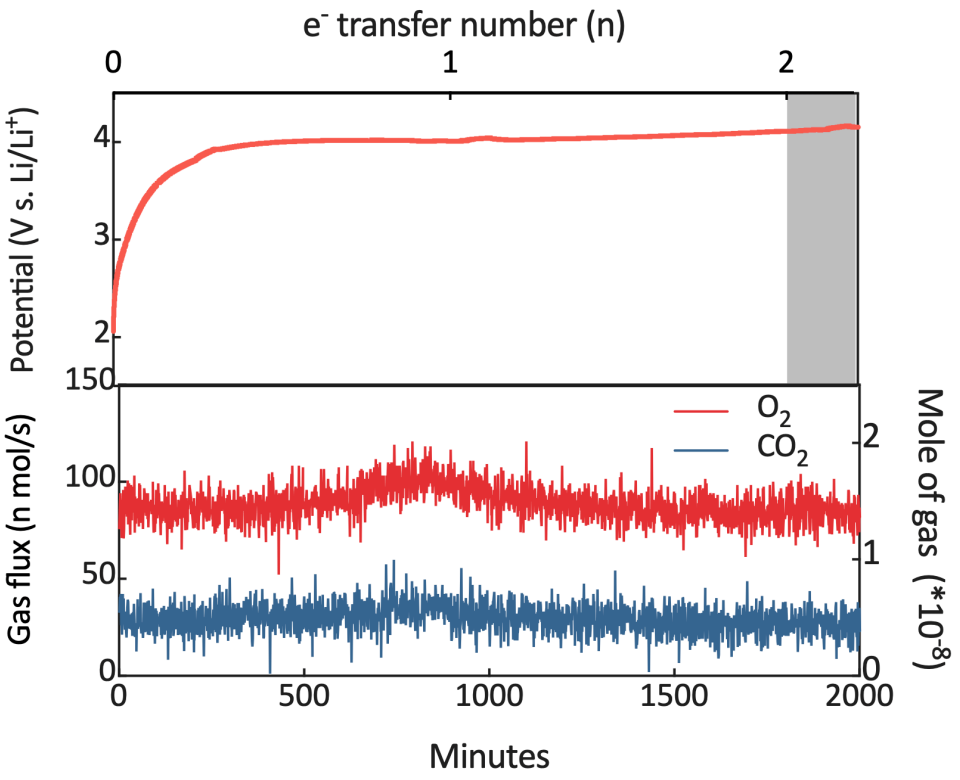

Figure 5. Top: Galvanostatic charge profile of the CaCoSO electrode acquired at a rate of 0.05C (1C rate corresponds to 365 mA g^{-1}, or 1 Ca^{2+} exchanged in one hour), the portion exceeding the theoretical capacity has been highlighted with a gray background in the figures, using Li counter and pseudo-reference electrode and LP57 as electrolyte. Bottom: Constant current step DEMS measurements for CO_2, and O_2 evolution.

We also conducted DEMS analysis, as well as extracted the electrolyte from cycled cells and analyzed the metal content by ICP-OES for the CaCoSO-AC cell configuration, employing 0.5M $Ca(TFSI)_2$ in EC/PC (1:1) as electrolyte. **Figure 6** displays the charge and discharge

process along with gas generation rate for CO_2 at m/z = 44, O_2 at m/z = 32, and H_2 at m/z = 2. The entire charge-discharge process can be divided into three stages. Stage I involves the release of primarily O_2, corresponding to the onset of CaCoSO decomposition as discussed earlier. In stage II, a significant increase in CO_2 evolution is noted at the beginning, indicating the decomposition of EC or PC solvents. This behavior differs from the one using LP57 electrolyte wherein CO_2 generation rate remained constant throughout the charging process (**Figure 5**). In the study by Freunberger et al.[44], it was demonstrated that the decomposition of PC in the presence of reactive oxygen species does not require high voltages, with a similar phenomenon potentially occurring in our system, with the observed rapid increase in CO_2 generation rate when the cell polarization reached 1.1 V. This is likely due to the accumulation of generated oxygen in the system, combined with the electrocatalytic effects, which create favorable conditions for PC decomposition. By comparing the electrolyte composition extracted at the beginning and end of the charging process by ICP-OES, a significant increase in calcium content is also noted (**Table S5**). Based on results obtained using the LP57 electrolyte in the same system, the calcium and cobalt content released from CaCoSO decomposition were found to be of the same order of magnitude (**Table S4**). However, in this system, the rise in calcium content cannot be solely attributed to the decomposition of CaCoSO. This strongly suggests that catalytic decomposition of the electrolyte also occurs in the Ca-ion electrolyte system. (**Figure S11, Table S5**).

Upon transitioning to the discharge step in stage III, a significant amount of H_2 release is noted, particularly for cell voltage below -1V (**Figure 6**). Considering the inert nature of the

counter-electrode (AC in this case) this process should relate to a cathodic reaction taking place at the CaCoSO positive electrode during discharge. Amongst the possible degradation routes that can generate cathodically H_2, while also considering the rather mild reduction conditions attained (-1V to -2V, vs. AC), this can be most reasonably associated to the decomposition of H_2O, as the release rate (the slope of line in stage III of **Figure 6 Bottom**) of O_2 is about half that of H_2. Since coulometric analysis of the initial electrolyte indicated a water content less than 10 ppm, the water is identified here as the byproduct of the catalytic decomposition of the electrolyte during the charge step. In lithium-oxygen systems, water was also shown to be produced as a side reaction during charging due to the carbonate solvents being susceptible to nucleophilic attack or proton abstraction by active O_2 radicals.[44–46] In the particular case of this study, decomposition of CaCoSO during charging, could also proceed (partially, or fully) through anion redox, and thus superoxide or singlet oxygen to be produced, reacting with the electrolyte solvent (EC or PC) to produce water.(**Figure S11, Table S5**). Although detailed mechanism of CaCoSO and electrolyte decomposition remains complex to unveil, requiring further studies, possible degradation pathways are schematically presented in **Figure S12**.

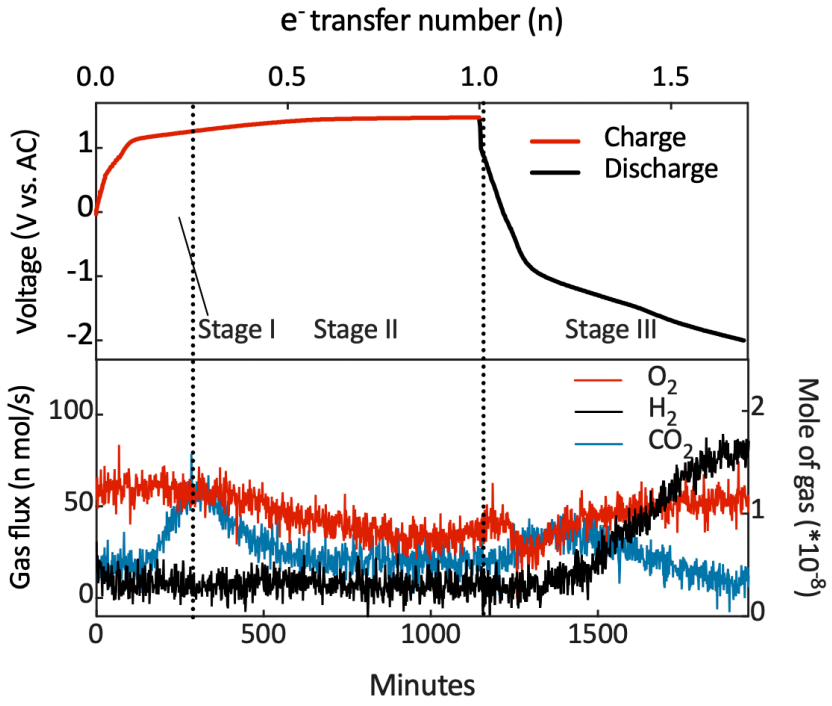

Figure 6. Top: Galvanostatic charge-discharge profile of CaCoSO electrode acquired at a rate of 0.05C (1C rate corresponds to 365 mA g^{-1}, or 1Ca^{2+} exchanged in one hour), in CaCoSO-AC cell configuration, using $Ca(TFSI)_2$ in EC/PC(1:1) as electrolyte. Bottom: Constant current step DEMS measurements for CO_2, O_2, and H_2 evolution.

As observed with other Ca-host compounds, similar galvanostatic charge and discharge characteristics to that of CaCoSO, especially the plateaus at the end of the charging curve, can be also noted. The galvanostatic charge step profile, corresponding to the Ca-ion extraction capacity, can be indeed related to a partial phase change or conversion, although precise quantification is required. Consequently, the discharge capacity is considered to be due to the ion storage capacity of the material. Our study, although remaining specific to this particular CaCoSO chemistry, highlights that one possible explanation for the discharge plateau formation, can be due to the material decomposition, triggering the decomposition of the

electrolyte. Herein, the oxidative decomposition, as well as electrocatalytic effect of CaCoSO during the charge step are found to generate water (alike already noted in metal-O_2 systems), with the subsequent decomposition resulting in H_2 generation, and the Coulombic charge consumed inevitably included as part of the discharge step capacity. This process can hinder the objective evaluation of material performance, presenting a potential challenge for future Ca electrode materials development.

CONCLUSION

In the pursuit of next-generation calcium-metal batteries (CMBs), the development of efficient and stable calcium-ion storage hosts remains a critical challenge. This work evaluates the Ca-storage performances of CaCoSO, a phase predicted to enable sequential Co^{2+}/Co^{3+} and Co^{3+}/Co^{4+} redox activity. Experimental results reveal that while theoretical capacity extraction can be effectively achieved, the underlying mechanism is dominated by material decomposition and electrolyte degradation rather than reversible Ca^{2+} uptake and release. *In situ* XRD and DEMS analyses demonstrated that these processes result in apparent charge-discharge plateaus, which are not associated with genuine ion storage but rather with side reactions, including catalytic decomposition of the carbonate-based electrolyte, water formation, and subsequently H_2 cathodic generation. These findings underscore the inherent complexities and pitfalls in evaluating divalent cation storage materials, particularly the need

to critically assess apparent performance metrics in the context of side reactions and non-reversible processes. Furthermore, the observed artifacts are consistent with challenges noted for other calcium-host systems, emphasizing the broader relevance of these phenomena in the field. This study highlights the necessity for advanced experimental validation, rigorous testing conditions, and appropriate design strategies to overcome the limitations of current materials and develop high-performance CMBs. By exposing these limitations, this work provides a framework for guiding future research efforts and advancing calcium-based energy storage technologies.

Corresponding Author

Alexandru Vlad – Institute of Condensed Matter and Nanosciences, Université Catholique de Louvain, 1348 Louvain-la-Neuve, Belgium; Email: alexandru.vlad@uclouvain.be

Author Contributions

The manuscript was written through contributions of all authors. All authors have given approval to the final version of the manuscript. ‡These authors contributed equally.

Funding Sources

This work was supported by FWO and F.R.S.-FNRS under the Excellence of Science (EOS) program - ECOBAT [40007515]. D.T., M.D., Z.L., X.G. H.X., Y.Z., and F.X. acknowledges CSC for the PhD fellowship. B.V.R, D.R. and X.L acknowledge F.R.S.-FNRS for Chargé de Recherché (CR) fellowship (grant agreement No. 40023657, 1.B.098.23 and 40010559). X.L. acknowledges partial financial support from the Marie Skłodowska-Curie Actions (grant agreement No. 101064286) for his postdoctoral fellowship. R.M. acknowledges F.R.S.-FNRS for the Aspirant fellowship (grant agreement No. 1.A.836.23).

Notes

The data that support the findings of this study are available from the corresponding author upon reasonable request.

Supporting Information

Supporting Information is available from the ACS Online Library or from the authors.

The Supporting Information provides additional details on XRD refinement, electrochemical test results of CaCoSO-AC and CaCoSO-Li in different electrolytes, SEM images of CaCoSO before and after cycling, XPS analysis of CaCoSO before and after cycling, a comparison of XRD patterns for CaCoSO before and after chemical oxidation, ICP-OES results of the electrolyte extracted during cycling, and schematic diagram of the reaction of CaCoSO-AC during cycling.

REFERENCES

(1) Duffner, F.; Kronemeyer, N.; Tübke, J.; Leker, J.; Winter, M.; Schmuch, R. Post-Lithium-Ion Battery Cell Production and Its Compatibility with Lithium-Ion Cell Production Infrastructure. *Nat Energy* **2021**, *6* (2), 123–134. https://doi.org/10.1038/s41560-020-00748-8.

(2) Liang, Y.; Dong, H.; Aurbach, D.; Yao, Y. Current Status and Future Directions of Multivalent Metal-Ion Batteries. *Nat Energy* **2020**, *5* (9), 646–656. https://doi.org/10.1038/s41560-020-0655-0.

(3) Whittingham, M. S. Lithium Batteries and Cathode Materials. *Chem. Rev.* **2004**, *104* (10), 4271–4302. https://doi.org/10.1021/cr020731c.

(4) Li, M.; Lu, J.; Chen, Z.; Amine, K. 30 Years of Lithium-Ion Batteries. *Advanced Materials* **2018**, *30* (33), 1800561. https://doi.org/10.1002/adma.201800561.

(5) Bruce, P. G.; Freunberger, S. A.; Hardwick, L. J.; Tarascon, J.-M. Li–O_2 and Li–S Batteries with High Energy Storage. *Nature Mater* **2012**, *11* (1), 19–29. https://doi.org/10.1038/nmat3191.

(6) Kim, T.; Song, W.; Son, D.-Y.; Ono, L. K.; Qi, Y. Lithium-Ion Batteries: Outlook on Present, Future, and Hybridized Technologies. *J. Mater. Chem. A* **2019**, *7* (7), 2942–2964. https://doi.org/10.1039/C8TA10513H.

(7) Ji, B.; He, H.; Yao, W.; Tang, Y. Recent Advances and Perspectives on Calcium-Ion Storage: Key Materials and Devices. *Advanced Materials* **2021**, *33* (2), 2005501. https://doi.org/10.1002/adma.202005501.

(8) Tian, Y.; Zeng, G.; Rutt, A.; Shi, T.; Kim, H.; Wang, J.; Koettgen, J.; Sun, Y.; Ouyang, B.; Chen, T.; Lun, Z.; Rong, Z.; Persson, K.; Ceder, G. Promises and Challenges of Next-Generation "Beyond Li-Ion" Batteries for Electric Vehicles and Grid Decarbonization. *Chem. Rev.* **2021**, *121* (3), 1623–1669. https://doi.org/10.1021/acs.chemrev.0c00767.

(9) Hosein, I. D. The Promise of Calcium Batteries: Open Perspectives and Fair Comparisons. *ACS Energy Lett.* **2021**, *6* (4), 1560–1565. https://doi.org/10.1021/acsenergylett.1c00593.

(10) Ponrouch, A.; Frontera, C.; Bardé, F.; Palacín, M. R. Towards a Calcium-Based Rechargeable Battery. *Nature Mater* **2016**, *15* (2), 169–172. https://doi.org/10.1038/nmat4462.

(11) Wang, D.; Gao, X.; Chen, Y.; Jin, L.; Kuss, C.; Bruce, P. G. Plating and Stripping Calcium in an Organic Electrolyte. *Nature Mater* **2018**, *17* (1), 16–20. https://doi.org/10.1038/nmat5036.

(12) Forero-Saboya, J.; Davoisne, C.; Dedryvère, R.; Yousef, I.; Canepa, P.; Ponrouch, A. Understanding the Nature of the Passivation Layer Enabling Reversible Calcium Plating. *Energy & Environmental Science* **2020**, *13* (10), 3423–3431. https://doi.org/10.1039/D0EE02347G.

(13) Wu, Y.; Zhao, Z.; Hao, X.; Xu, R.; Li, L.; Lv, D.; Huang, X.; Zhao, Q.; Xu, Y.; Wu, Y. Cathode Materials for Calcium-Ion Batteries: Current Status and Prospects. *Carbon Neutralization* **2023**, *2* (5), 551–573. https://doi.org/10.1002/cnl2.85.

(14) Hua, Y.; Ma, Y.; Qi, Q.; Xu, Z.-L. Cathode Materials for Non-Aqueous Calcium Rechargeable Batteries. *Nanoscale* **2024**. https://doi.org/10.1039/D4NR02966F.

(15) Xie, J.; Zhang, Q. Recent Progress in Multivalent Metal (Mg, Zn, Ca, and Al) and Metal-Ion Rechargeable Batteries with Organic Materials as Promising Electrodes. *Small* **2019**, *15* (15), 1805061. https://doi.org/10.1002/smll.201805061.

(16) Yu, X.; Boyer, M. J.; Hwang, G. S.; Manthiram, A. Toward a Reversible Calcium-Sulfur Battery with a Lithium-Ion Mediation Approach. *Advanced Energy Materials* **2019**, *9* (14), 1803794. https://doi.org/10.1002/aenm.201803794.

(17) Li, Z.; Vinayan, B. P.; Jankowski, P.; Njel, C.; Roy, A.; Vegge, T.; Maibach, J.; Lastra, J. M. G.; Fichtner, M.; Zhao-Karger, Z. Multi-Electron Reactions Enabled by Anion-Based Redox Chemistry for High-Energy Multivalent Rechargeable Batteries. *Angewandte Chemie International Edition* **2020**, *59* (28), 11483–11490. https://doi.org/10.1002/anie.202002560.

(18) Zhou, R.; Hou, Z.; Fan, K.; Wun, C. K.; Liu, Q.; Benedict Lo, T. W.; Huang, H.; Zhang, B. An Advanced Organic Cathode for Non-Aqueous and Aqueous Calcium-Based Dual Ion Batteries. *Journal of Power Sources* **2023**, *569*, 232995. https://doi.org/10.1016/j.jpowsour.2023.232995.

(19) Okamoto, S.; Ichitsubo, T.; Kawaguchi, T.; Kumagai, Y.; Oba, F.; Yagi, S.; Shimokawa, K.; Goto, N.; Doi, T.; Matsubara, E. Intercalation and Push-Out Process with Spinel-to-Rocksalt Transition on Mg Insertion into Spinel Oxides in Magnesium Batteries. *Advanced Science* **2015**, *2* (8), 1500072. https://doi.org/10.1002/advs.201500072.

(20) Liu, M.; Rong, Z.; Malik, R.; Canepa, P.; Jain, A.; Ceder, G.; A. Persson, K. Spinel Compounds as Multivalent Battery Cathodes: A Systematic Evaluation Based on Ab Initio Calculations. *Energy & Environmental Science* **2015**, *8* (3), 964–974. https://doi.org/10.1039/C4EE03389B.

(21) Torres, A.; Arroyo-de Dompablo, M. E. Comparative Investigation of $MgMnSiO_4$ and Olivine-Type $MgMnSiS_4$ as Cathode Materials for Mg Batteries. *J. Phys. Chem. C* **2018**, *122* (17), 9356–9362. https://doi.org/10.1021/acs.jpcc.8b02369.

(22) Dompablo, M. E. A.; Krich, C.; Nava-Avendaño, J.; Palacín, M. R.; Bardé, F. In Quest of Cathode Materials for Ca Ion Batteries: The $CaMO_3$ Perovskites (M = Mo, Cr, Mn, Fe, Co, and Ni). *Phys. Chem. Chem. Phys.* **2016**, *18* (29), 19966–19972. https://doi.org/10.1039/C6CP03381D.

(23) Sai Gautam, G.; Canepa, P.; Malik, R.; Liu, M.; Persson, K.; Ceder, G. First-Principles Evaluation of Multi-Valent Cation Insertion into Orthorhombic V_2O_5. *Chemical Communications* **2015**, *51* (71), 13619–13622. https://doi.org/10.1039/C5CC04947D.

(24) Tchitchekova, D. S.; Frontera, C.; Ponrouch, A.; Krich, C.; Bardé, F.; Palacín, M. R. Electrochemical Calcium Extraction from 1D-$Ca_3Co_2O_6$. *Dalton Trans.* **2018**, *47* (33), 11298–11302. https://doi.org/10.1039/C8DT01754A.

(25) Tchitchekova, D. S.; Ponrouch, A.; Verrelli, R.; Broux, T.; Frontera, C.; Sorrentino, A.; Bardé, F.; Biskup, N.; Arroyo-de Dompablo, M. E.; Palacín, M. R. Electrochemical Intercalation of Calcium and Magnesium in TiS_2: Fundamental Studies Related to Multivalent Battery Applications. *Chem. Mater.* **2018**, *30* (3), 847–856. https://doi.org/10.1021/acs.chemmater.7b04406.

(26) Canepa, P.; Sai Gautam, G.; Hannah, D. C.; Malik, R.; Liu, M.; Gallagher, K. G.; Persson, K. A.; Ceder, G. Odyssey of Multivalent Cathode Materials: Open Questions and Future Challenges. *Chem. Rev.* **2017**, *117* (5), 4287–4341. https://doi.org/10.1021/acs.chemrev.6b00614.

(27) Ceder, G. Predicting Properties from Scratch. *Science* **1998**, *280* (5366), 1099–1100. https://doi.org/10.1126/science.280.5366.1099.

(28) Juran, T. R.; Smeu, M. Hybrid Density Functional Theory Modeling of Ca, Zn, and Al Ion Batteries Using the Chevrel Phase Mo_6S_8 Cathode. *Phys. Chem. Chem. Phys.* **2017**, *19* (31), 20684–20690. https://doi.org/10.1039/C7CP03378H.

(29) Black, A. P.; Frontera, C.; Torres, A.; Recio-Poo, M.; Rozier, P.; Forero-Saboya, J. D.; Fauth, F.; Urones-Garrote, E.; Arroyo-de Dompablo, M. E.; Palacín, M. R. Elucidation of the Redox Activity of $Ca_2MnO_{3.5}$ and CaV_2O_4 in Calcium Batteries Using Operando XRD: Charge Compensation Mechanism and Reversibility. *Energy Storage Materials* **2022**, *47*, 354–364. https://doi.org/10.1016/j.ensm.2022.02.017.

(30) P. Black, A.; Torres, A.; Frontera, C.; Rosa Palacín, M.; Dompablo, M. E. A. Appraisal of Calcium Ferrites as Cathodes for Calcium Rechargeable Batteries: DFT, Synthesis, Characterization and Electrochemistry of $Ca_4Fe_9O_{17}$. *Dalton Transactions* **2020**, *49* (8), 2671–2679. https://doi.org/10.1039/C9DT04688G.

(31) Torres, A.; Casals, J. L.; Arroyo-de Dompablo, M. E. Enlisting Potential Cathode Materials for Rechargeable Ca Batteries. *Chem. Mater.* **2021**, *33* (7), 2488–2497. https://doi.org/10.1021/acs.chemmater.0c04741.

(32) Gorbunov, M. V.; Carrocci, S.; Maletti, S.; Valldor, M.; Doert, T.; Hampel, S.; Gonzalez Martinez, I. G.; Mikhailova, D.; Gräßler, N. Synthesis of $(Li_2Fe_{1-y}Mn_y)SO$ Antiperovskites with Comprehensive Investigations of $(Li_2Fe_{0.5}Mn_{0.5})SO$ as Cathode in Li-Ion Batteries. *Inorg. Chem.* **2020**, *59* (21), 15626–15635. https://doi.org/10.1021/acs.inorgchem.0c01753.

(33) Gamon, J.; J. Perez, A.; H. Jones, L. A.; Zanella, M.; M. Daniels, L.; E. Morris, R.; C. Tang, C.; D. Veal, T.; J. Hardwick, L.; S. Dyer, M.; B. Claridge, J.; J. Rosseinsky, M. $Na_2Fe_2OS_2$, a New Earth Abundant Oxysulphide Cathode Material for Na-Ion Batteries. *Journal of Materials Chemistry A* **2020**, *8* (39), 20553–20569. https://doi.org/10.1039/D0TA07966A.

(34) Hailemariam, A. G.; Syum, Z.; Mamo, T. T.; Qorbani, M.; Hsing, C.-R.; Sabbah, A.; Quadir, S.; Bayikadi, K. S.; Wu, H.-L.; Wei, C.-M.; Chen, L.-C.; Chen, K.-H. Oxygen-Incorporated Lithium-Rich Iron Sulfide Cathodes for Li-Ion Batteries with Boosted Material Stability and Electrochemical Performance. *Chem. Mater.* **2024**, *36* (19), 9370–9379. https://doi.org/10.1021/acs.chemmater.4c00508.

(35) Zak, J. J.; Kim, S. S.; Laskowski, F. A. L.; See, K. A. An Exploration of Sulfur Redox in Lithium Battery Cathodes. *J. Am. Chem. Soc.* **2022**, *144* (23), 10119–10132. https://doi.org/10.1021/jacs.2c02668.

(36) Zhu, Q.; Wang, J.; Liu, X.; Ebejer, N.; Rambabu, D.; Vlad, A. Mixed Anionic and Cationic Redox Chemistry in a Tetrathiomolybdate Amorphous Coordination Framework. *Angewandte Chemie* **2020**, *132* (38), 16722–16729. https://doi.org/10.1002/ange.202004587.

(37) Salter, E. J. T.; Blandy, J. N.; Clarke, S. J. Crystal and Magnetic Structures of the Oxide Sulfides CaCoSO and BaCoSO. *Inorg. Chem.* **2016**, *55* (4), 1697–1701. https://doi.org/10.1021/acs.inorgchem.5b02615.

(38) Li, Z.; Li, Y.; Zhan, Y.; Lin, X.; Yao, Y.; Zhao, T.; Sun, F.; Xu, H.; Ma, Z.; Zhang, W.; Xue, Y.; Li, X.; Vlad, A.; Zou, J. On the Origin of Capacity Increase in Rechargeable Magnesium Batteries with Manganese Oxide Cathodes and Copper Metal Current Collectors. *Angewandte Chemie International Edition* **2024**, e202416960. https://doi.org/10.1002/anie.202416960.

(39) Wizansky, A. R.; Rauch, P. E.; Disalvo, F. J. Powerful Oxidizing Agents for the Oxidative Deintercalation of Lithium from Transition-Metal Oxides. *Journal of Solid State Chemistry* **1989**, *81* (2), 203–207. https://doi.org/10.1016/0022-4596(89)90007-8.

(40) Lipson, A. L.; Proffit, D. L.; Pan, B.; Fister, T. T.; Liao, C.; Burrell, A. K.; Vaughey, J. T.; Ingram, B. J. Current Collector Corrosion in Ca-Ion Batteries. *J. Electrochem. Soc.* **2015**, *162* (8), A1574–A1578. https://doi.org/10.1149/2.0811508jes.

(41) Mahne, N.; Renfrew, S. E.; McCloskey, B. D.; Freunberger, S. A. Electrochemical Oxidation of Lithium Carbonate Generates Singlet Oxygen. *Angewandte Chemie International Edition* **2018**, *57* (19), 5529–5533. https://doi.org/10.1002/anie.201802277.

(42) Wang, H.; Rus, E.; Sakuraba, T.; Kikuchi, J.; Kiya, Y.; Abruña, H. D. CO_2 and O_2 Evolution at High Voltage Cathode Materials of Li-Ion Batteries: A Differential Electrochemical Mass Spectrometry Study. *Anal. Chem.* **2014**, *86* (13), 6197–6201. https://doi.org/10.1021/ac403317d.

(43) Han, J.-G.; Kim, K.; Lee, Y.; Choi, N.-S. Scavenging Materials to Stabilize LiPF6-Containing Carbonate-Based Electrolytes for Li-Ion Batteries. *Advanced Materials* **2019**, *31* (20), 1804822. https://doi.org/10.1002/adma.201804822.

(44) Freunberger, S. A.; Chen, Y.; Peng, Z.; Griffin, J. M.; Hardwick, L. J.; Bardé, F.; Novák, P.; Bruce, P. G. Reactions in the Rechargeable Lithium–O2 Battery with Alkyl Carbonate Electrolytes. *J. Am. Chem. Soc.* **2011**, *133* (20), 8040–8047. https://doi.org/10.1021/ja2021747.

(45) Gao, X.; Chen, Y.; Johnson, L.; Bruce, P. G. Promoting Solution Phase Discharge in Li–O2 Batteries Containing Weakly Solvating Electrolyte Solutions. *Nature Mater* **2016**, *15* (8), 882–888. https://doi.org/10.1038/nmat4629.

(46) Black, R.; Oh, S. H.; Lee, J.-H.; Yim, T.; Adams, B.; Nazar, L. F. Screening for Superoxide Reactivity in Li-O2 Batteries: Effect on Li2O2/LiOH Crystallization. *J. Am. Chem. Soc.* **2012**, *134* (6), 2902–2905. https://doi.org/10.1021/ja2111543.

Figure TOC

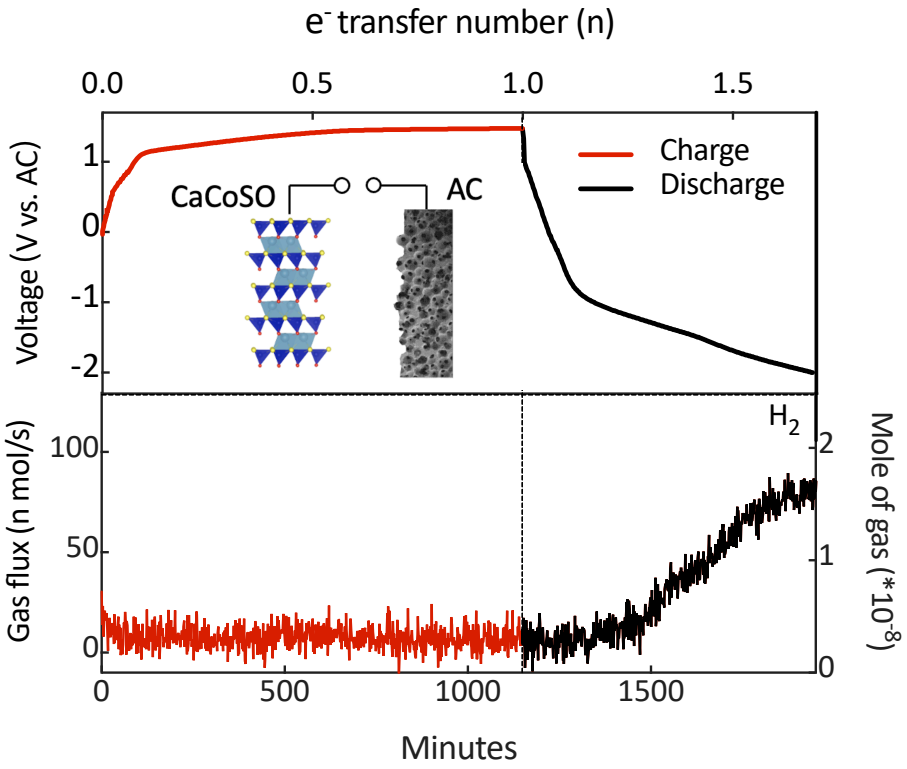
e- transfer number (n)
0.0
0.5
1.0
1.5
Voltage (V vs. AC)
1
0
-1
-2
CaCoSO
AC
Charge
Discharge
Gas flux (n mol/s)
100
50
0
H2
Mole of gas (*10-8)
2
1
0
0
500
1000
1500
Minutes